Progress In Electromagnetics Research C, Vol. 80, 181–198, 2018

A Novel High Directive Willis-Sinha Tapered Slot Antenna for GPR Application in Detecting Landmine

Mohammed M. Mohanna[1, *], Esmat A. Abdallah[2], Hadia M. Elhennawy[3], and Magdy M. Kamel[4]

Abstract—A novel Ultra-wideband Willis-Sinha Tapered Slot antenna for landmine detection using Ground Penetrating Radar (GPR) system with enhanced gain and directivity is presented. The structure is constructed on a $235 \times 270\,\text{mm}^2$ FR4 dielectric substrate. The antenna is fed by a novel tapered coplanar waveguide (CPW) to coplanar stripline (CPS) transition feed. The antenna's impedance bandwidth is extended by adding an antenna arm constructing parabola shape with the antenna element. The antenna has a corrugated structure along the antenna outer edges to improve radiation efficiency and get higher directivity. Also, a mushroom-like circular EBG structure is used in the lower side of the antenna arm to reduce interference and enhance front-to-back ratio (F/B ratio). A partial substrate removal, like circular cylinders inside the substrate, is aligned with the antenna tapered profile to obtain better radiation efficiency and enhance antenna gain. The operational bandwidth of this antenna extends from 0.18 to 6.2 GHz. The minimum return loss reaches 60 dB. The average directivity reaches 12.2 dBi while the gain and radiation efficiency are 11.8 dBi and 92%, respectively with gain enhancement of 195% due to using corrugated structure and air cavities. The front-to-back ratio (F/B ratio) is 23 dB. Also, a size reduction of 48% is achieved due to using extended arm. The antenna performance was simulated and measured. Good agreement was found between numerical and experimental results. The proposed antenna is suitable for various ultra-wideband applications especially in landmine detection. The design of the proposed antenna is given in very simple five design steps.

1. INTRODUCTION

Landmine crisis is creating massive social and economic problems worldwide [1–3]. GPR is used as an efficient sensor to detect buried landmines. In this case, GPR antenna(s) must be lifted up above the ground [4, 5]. This requirement results in some propagation problems known as surface clutter, particularly when the ground is rough [4–7]. In the case of low contrast in electromagnetic properties of the buried objects near-surface and their surrounding soil besides, the contribution of ground surface clutter (soil conditions and/or surface roughness) will lead to corruption for the reflected signals, and uncertainty in the measurements may occur [4]. The detection of the buried object located near the ground surface as well as small and low-contrast landmines needs to use higher frequencies to achieve a better resolution [4].

The tapered slot antenna (TSA) attracts much attention in GPR application due to its low cost, low weight, simple fabrication, compactness, wideband properties and end-fire radiation. A compact TSA for GPR applications, which has large bandwidth and small size, is proposed in [8].

Introducing the Willis-Sinha taper is quite a challenge as more size reduction, larger bandwidth and higher antenna gain have been achieved than the exponential one, besides, more stable in the energy

Received 19 November 2017, Accepted 12 January 2018, Scheduled 22 January 2018

* Corresponding author: Mohammed Mahmoud Mohanna (mohanna_2085@hotmail.com).

[1] Ministry of Electricity & Renewable Energy, Abbassia, Cairo, Egypt. [2] Electronics Research Institute, Dokki, Giza, Egypt. [3] Faculty of Engineering, Ain Shams University, Cairo, Egypt. [4] National Research Institute of Astronomy and Geophysics, Egypt.

reflection. The comparison between Willis-Sinha and exponential tapers in [9, 10] is taken as a guide for the tapered slots design. Transition structures are employed to transform electromagnetic energy between two different types of transmission lines as they achieve smooth transition, in impedance and field matching. Coplanar waveguide (CPW) is unbalanced and can be directly connected to unbalanced coaxial cable. If this combination is to be used, a transition from CPW to CPS should be implemented to accomplish the unbalanced to balanced transformation and enhance matching [11].

As known, the aperture width of a TSA should be at least half-wavelength at the lowest operating frequency in free space, so for low-frequency applications such as GPR, it may require large size of TSA. In order to expand the band to lower frequency, the arms of the antenna are rolled back as a long current path occurs [12]. The corrugated structure can improve the radiation pattern and antenna gain of the Vivaldi antenna, and better front-to-back ratio can be achieved [13–16]. Removing some parts from substrate surrounding the antenna radiating element will also increase the antenna gain [17].

In this paper, a novel high directive Willis-Sinha Tapered Slot Antenna with high directivity is presented; there are some modifications on the antenna geometry firstly, using Willis-Sinha tapered profile rather than using the exponential tapering. Furthermore, a novel planar coplanar waveguide (CPW) to coupled stripline (CPS) transition is modified and designed. Secondly, the antenna arm is elongated and rolled back, and a corrugated structure along the outer edges making an ellipse shape with the antenna outer edge and the elongated arm and mushroom-like EBG structure near the arm are used to reduce the loading due to the elongated arm. Lastly, a partial substrate removal, like circular cavities inside the substrate, is aligned with the tapering profile and antenna outer edge to increase antenna gain and directivity. All of these modifications affect more on enhancing antenna gain and directivity. The simulations were done using CST ver. 15.

The paper is organized as follows: Section 2 presents the final antenna geometry, while Section 3 introduces the proposed antenna design steps. Designing the symmetric tapered slot antenna, designing the asymmetric coplanar slot line, designing the CPW to CPS transition, adding rolled back elongated arm and the corrugated structures, etching air cavities inside the substrates and studying the effect of each design step on return loss, antenna gain and radiation efficiency in order to reach the optimum design parameters. A comparison between simulation and measured data has been done. Section 4 gives the conclusion.

2. ANTENNA GEOMETRY

Figure 1 shows the configuration of the proposed Willis Sinha tapered slot antenna with high gain. The proposed antenna is constructed on an FR4 substrate with $W_{\text{sub}} \times L_{\text{sub}} = 270 \times 235\,\text{mm}^2$, thickness $h = 1.5\,\text{mm}$, relative dielectric constant of 4.65, and $\tan\delta$ of 0.03. The main part of the antenna is a Willis-Sinha tapered configuration, and the size of this part is $W_{\text{slot}} \times L_{\text{slot}} = 94 \times 191\,\text{mm}^2$. The remaining part CPW-fed CPS with UWB performance with $W_{g1} = W_{g2} = 93\,\text{mm}$, $L_{th} = 44\,\text{mm}$, $S = 1.5\,\text{mm}$, $g = 1.9\,\text{mm}$, $R_1 = 42\,\text{mm}$ and $R_2 = 81\,\text{mm}$. A smoothly rolled back arms length $L_{\text{arm}} = 195\,\text{mm}$ with $A = 120\,\text{mm}$ and $B = 69\,\text{mm}$ is presented where A and B are the major and minor axes of the ellipse. Besides, an EBG circular mushroom-like structure with radius $b = 10\,\text{mm}$, via pins with radius $r = 1\,\text{mm}$ and $P_1 = 23\,\text{mm}$ is located near the end of the rolled arm. The horizontal distance between the lower part of the antenna arm and the right-hand side of the ground is 70 mm. In this design, the corrugated edge structure is implemented by adding some slits in the antenna $L_a = 10\,\text{mm}$, $L_{s1} = 20\,\text{mm}$, $L_{s2} = 8\,\text{mm}$, $L_o = 2\,\text{mm}$ and $L_r = 8\,\text{mm}$, $W_r = 50\,\text{mm}$. The radius $a = 10\,\text{mm}$ of circular cavities and $P_2 = 26\,\text{mm}$. All simulations were performed in CST ver. 15. All the antenna dimensions are shown in Table 1. In the next section the antenna design steps will be discussed.

3. PROPOSED ANTENNA DESIGN STEPS AND DISCUSSION

The lack of a proven design procedure of adjustable antenna parameters leads to the development of the design methodology detailed below. The proposed design methodology serves as a guide to establish a starting point that can be made to optimize tapered slot antenna performance as shown in Fig. 1.

Selecting a substrate material is entirely dependent on operational bandwidth and budget. So, we select an FR-4 substrate for commercially low cost.

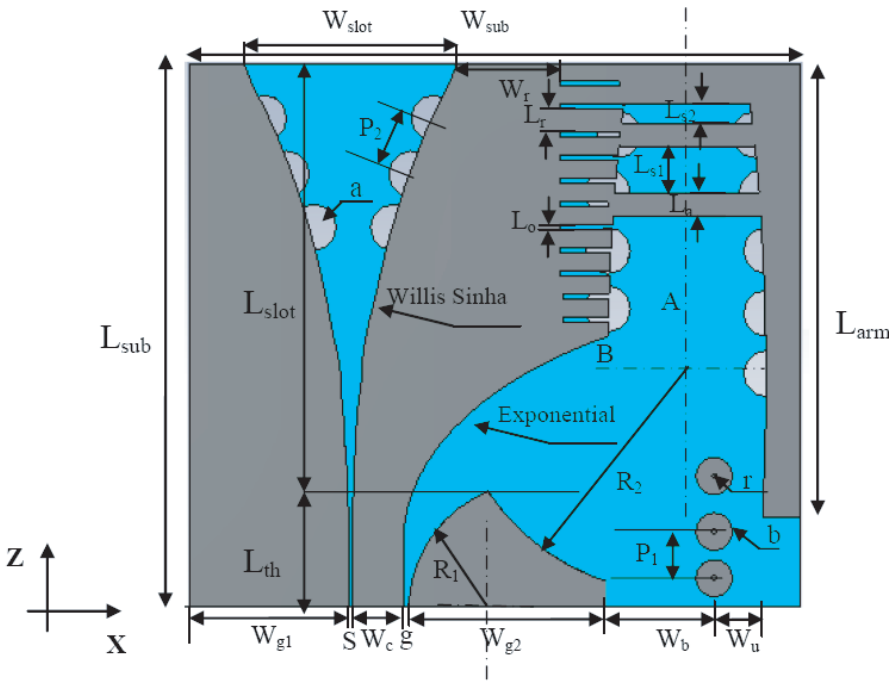

Figure 1. Geometry of the tapered slot line antenna with EBG structure.

Table 1. The proposed antenna dimension (all dimensions in mm).

W_{sub}	L_{sub}	Willis Sinha taper		Willis-Sinha taper rate
		W_{slot}	L_{slot}	$x = 94 * \exp\left\{-0.02 * \left(Z - 0.75 - \frac{0.2405}{2\pi}\sin\left(2\pi * Z\right)\right)\right\} - 94$
270	235	94	191	

CPW to CPS Transition						
$W_{g1} = W_{g2}$	W_c	L_{th}	S	G	R_1	R_2
93	23	44	1.5	1.9	42	81

Outer Exponential Rate: $23.75 * e^{0.03*Z^2}$													
Antenna Arm and EBG											Circular Cavities		
L_{arm}	A	B	L_a	L_{s1}	L_{s2}	L_o	L_r	W_r	b	R	A	$\mathbf{P_1}$	$\mathbf{P_2}$
195	120	69	10	20	8	2	8	50	10	1	10	23	26

The antenna design procedure is suggested according to the following steps:

(i) Designing a symmetric tapered slot antenna and studying the effect of the tapering type for both Exponential and Willis-Sinha tapers on antenna bandwidth and gain, Fig. 2(a). **(Assume that the left-hand side of the tapered slot antenna is grounded, and the right-hand side is the antenna radiating element).**

(ii) Constructing the asymmetric Coplanar Strip line CPS by partially removing the metal in the antenna radiating element and studying its effect on the antenna bandwidth, Fig. 2(b). Parametric study has been done on the antenna parameters to enhance the matching.

(iii) Designing the Coplanar Waveguide to Coplanar Strip "CPW to CPS" transition, Fig. 2(c), and studying the effect on the bandwidth and matching. Besides simple equivalent circuit for the transition is proposed.

(iv) Adding elongated rolled back arm in the antenna radiating element as well as the corrugated

structures and studying its effect on the bandwidth enhancement, Fig. 2(d). Besides the parametric study has been done on the antenna parameters.

(v) Etching circular cavities inside the substrate and studying its effect on the directivity, gain and radiation efficiency. Parametric study has been done on the antenna parameters.

Figure 2 shows the change in the antenna geometry during design steps.

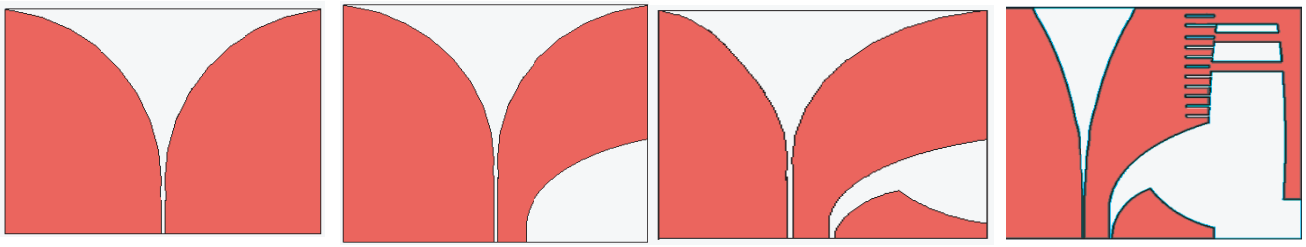

Figure 2. The changes in the antenna geometry during design steps. (a) The antenna symmetrical coplanar slot line. (b) Antenna asymmetric coplanar slot line. (c) Antenna with CPW to CPS transition. (d) Antenna with elongated arm and corrugated slits.

In the following sections the detailed design steps are discussed.

3.1. Designing the Symmetric Tapered Slot Antenna

Figure 3 shows the geometry of simple shape of the symmetric tapered slot antenna. The antenna has many parameters such as tapered slot width W_{slot}, slot length L_{slot}, throating length L_{th} and slot gap S. In order to calculate these parameters, antenna design requirements must be determined such as the operating frequency, minimum and maximum frequencies, and required gain. Besides, it depends in the GPR application whether it is used in landmine detection or ground water detection.

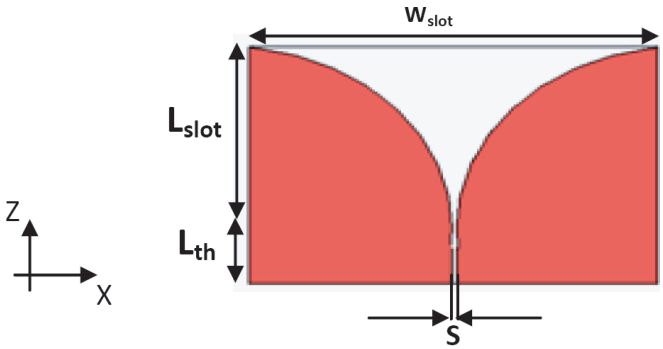

Figure 3. The simple shape of symmetrical tapered slot antenna.

3.1.1. Calculations

According to design requirements of the GPR antenna to detect both antitank and antipersonnel landmine, the required bandwidth is UWB, and it starts from $f_{\text{min}} = 0.4\,\text{GHz}$ to $f_{\text{max}} = 3\,\text{GHz}$ [3, 18].

There are some assumptions in our design:

(i) The required $f_{\text{min}} = 250\,\text{MHz}$ to achieve perfect matching when working at $f = 400\,\text{MHz}$.

(ii) The maximum width of the radiating element, which is the tapered slot, is chosen to be equal to effective half wavelength calculated at the lowest frequency of operation [9, 19].

(iii) The dielectric substrate is FR4 with thickness 1.5 mm, $\varepsilon_r = 4.65$ and $\tan\delta$ of 0.03, so the approximate effective dielectric constant is 2.78. Hence W_{slot} is 357 mm.

We can assume $W_{\text{slot}} = 350$ mm.

The slot width S can be calculated with 50 ohm input impedance matching [19] and is found to be 2 mm. The substrate width and length $W_{\text{sub}} \times L_{\text{sub}} = 35 \times 350\,\text{mm}^2$ are compatible with W_{slot}.

Assume $L_{th} = 70$ mm, then $L_{\text{slot}} = 280$ mm as an initial value before optimization.

The criteria of selection of tapering profile will be according to the optimization of the antenna gain and bandwidth.

3.2. Gain and Bandwidth for Exponential and Willis-Sinha Tapers

Comparison has been done between exponential tapered Slot and Willis- Sinha to study the effect on gain and bandwidth.

3.2.1. Exponential Tapered Slot

Assume that the approximate exponential tapering profile of the antenna is [9, 10, 19, 20]:

$$x = A\exp\left\{B * \left(Z - \frac{S}{2}\right)\right\} - A \qquad \text{for} \quad S/2 \le x \le W_{\text{slot}}/2 \tag{1}$$

$$A = L_{\text{slot}}/\{\exp\left(B\left[W_{\text{slot}} - S/2\right]\right) - 1\} \tag{2}$$

The selection for A is chosen such that the maximum opening of the TSA is constant and equal to W_{slot} for any value of the tapering profile parameter B, see Fig. 3. Note that for linear tapering $B = 0$ in Eq. (1).

For $W_{\text{sub}} = 350$ mm, $L_{\text{sub}} = 350$ mm, $W_{\text{slot}} = 350$ mm and $S = 2$ mm, the TSA performance was evaluated for different values of the tapering parameter B for FR4 substrate, using Matlab Program and CST studio ver. 15. The calculated values of the average gain and bandwidth are shown in Fig. 4. The result shows that the antenna has a maximum gain (1.95 dBi) when $B = 0.06$, and the maximum bandwidth is obtained when $B = -0.1$. When B is positive, the bandwidth and gain decrease. The optimum value for the parameter B is chosen as -0.035 (graphs intersection). Consequently $A = 280$ from Eq. (2) and the profile of the exponential tapered will be:

$$x = 280 * \exp\{-0.035 * (Z - 1)\} - 280 \tag{3}$$

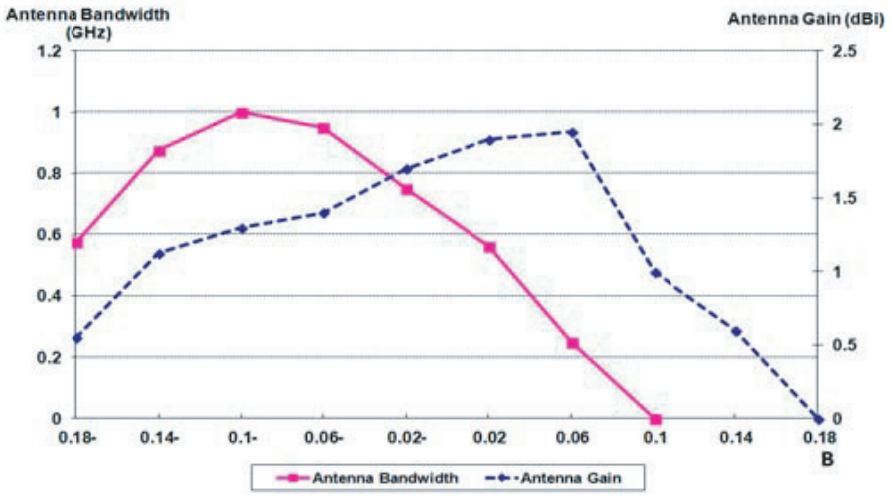

Figure 4. The Gain and Bandwidth variations versus tapering parameter B for ETSA.

3.2.2. Willis Sinha Tapered Slot

Again the same procedures are done for the Willis Sinha tapered slot [9, 10, 20]

$$x = A\exp\left\{B*\left(Z-\frac{S}{2}-\frac{0.2405}{2\pi}\sin(2\pi*Z)\right)\right\}-A \qquad for \quad S/2\le x\le W_{slot}/2 \tag{4}$$

$$A = L_{slot}/\left\{\exp\left[B*\left(W_{\text{slot}}-\frac{S}{2}-\frac{0.2405}{2\pi}\sin(2\pi*W_{\text{slot}})\right)\right]-1\right\} \tag{5}$$

The result in Fig. 5 indicates that the antenna has a maximum gain (2.85 dBi) when $B = -0.1$. The optimum value for the parameter B is chosen as -0.02 (graphs intersection). Then $A = 277$ from Eq. (5) and the equation of the Willis Sinha tapered antenna becomes:

$$x = 277*\exp\left\{-0.02*(Z-\frac{S}{2}-\frac{0.2405}{2\pi}\sin(2\pi*Z))\right\}-277 \tag{6}$$

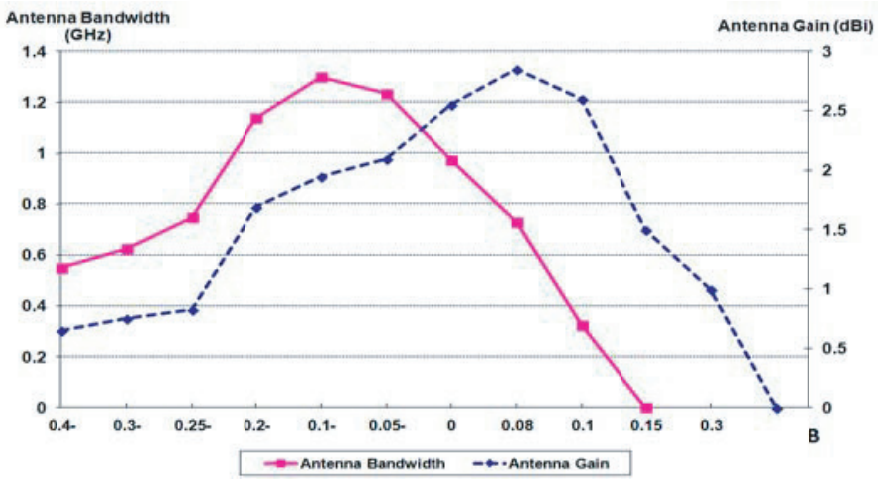

Figure 5. The gain and bandwidth variations versus tapering parameter B for Willis Sinha tapered slot antenna.

In conclusion as shown in Table 2 using Willis-Sinha tapering profile in the tapered slot antenna enhances antenna gain and bandwidth by 41% and 32%, respectively. So Willis-Sinha will be chosen as a tapering profile in the TSA.

Table 2. Comparison between exponential and Willis-Sinha tapered slot.

Antenna Taper profile	Exponential	Willis-Sinha	Diff. (%)
Max Bandwidth (GHz)	1	1.3	30
Max Gain (dBi)	1.95	2.85	46
Optimum Bandwidth (GHz)	0.77	1.15	49
Optimum Gain (dBi)	1.7	2.4	41

3.3. Designing the Asymmetric Coplanar Slot Line

The design of the asymmetric slot line feeder, as shown in Fig. 6, is done by making an opening exponential slot in the antenna element and study its effect on the antenna bandwidth and matching.

The outer opening is an exponential profile starting from P_3 $(x_3, z_3) = (25, 0)$ and ends at P_4 $(x_4, z_4) = (175, 97)$ with the following equation:

$$x = C_o * e^{K_o * Z^2} \tag{7}$$

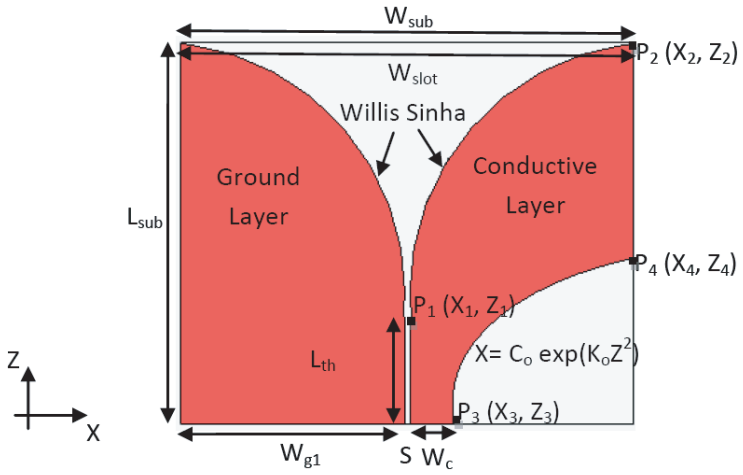

Figure 6. The geometry of the Asymmetric Coplanar Strip Line and Willis Sinha TSA.

where C_o is the distance from the center line of the slot to the outer tapered slot line $C_o = W_c + S/2$, and K_o determines the rate of the exponential outer slot.

The antenna was simulated in CST environment, and a parametric study has been done on W_c, S, L_{th}, C_o and K_o as shown in Figs. 7–10. For each step of the process, typical starting values are given. It is found that the optimum values are $W_c = 24\,\text{mm}$, $S = 2\,\text{mm}$, $L_{th} = 44\,\text{mm}$ and $K_o. = 0.03$.

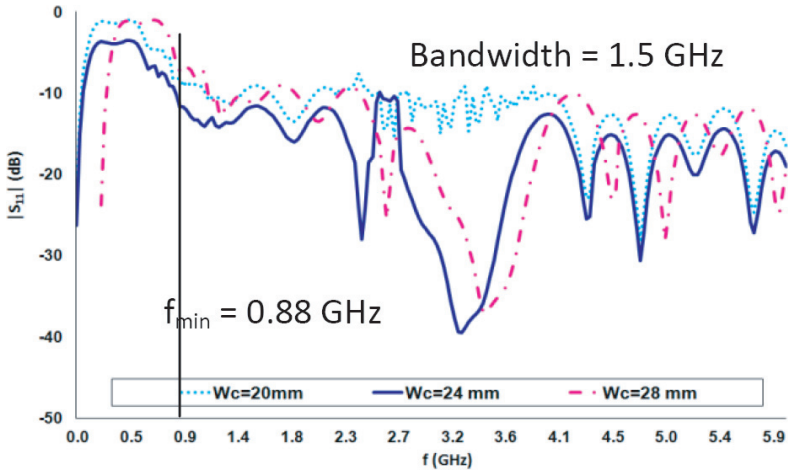

Figure 7. Effect of "W_c" on antenna bandwidth.

The bandwidth is increased from 0.99 GHz in symmetric strip line (Table 2) to 1.5 GHz in asymmetric strip line as shown in Figs. 7–10, with average antenna gain of about 4 dBi.

The dimension of the optimized parameters is shown in Table 3.

As shown in Table 3, the out exp rate and inner Willis Sinha rate are different as shown in Table 1 because the rates in Table 1 are calculated after design steps C & D.

Table 3. The optimized antenna parameters (All dimensions in mm).

Parameter	W_c	S	W_{g1}	L_{th}	Out Exp Rate	Inner Willis Sinha
Value	24	2	100	44	$25{*}e^{0.03{*}Z^2}$	$x = 277{*}\exp\left\{-0.02*\left(Z - \frac{S}{2} - \frac{0.2405}{2\pi}\sin(2\pi*Z)\right)\right\} - 277$

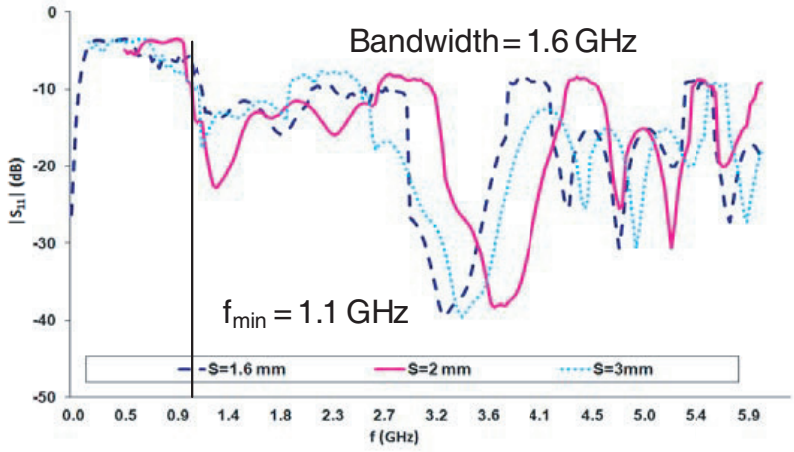

Figure 8. Effect of "S" on antenna bandwidth.

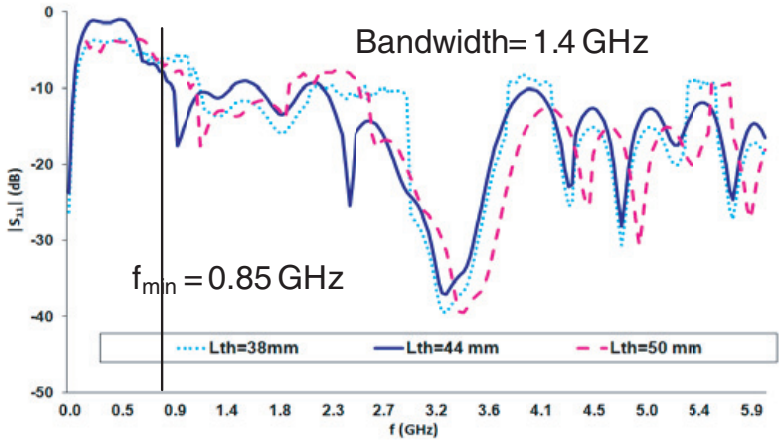

Figure 9. Effect of "L_{th}" on antenna bandwidth.

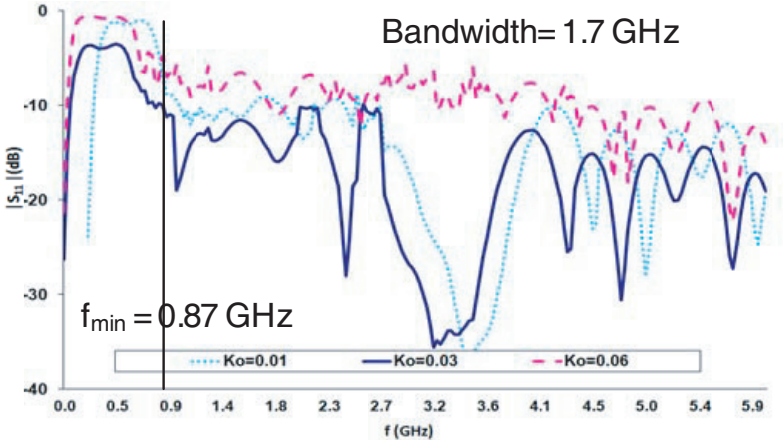

Figure 10. Effect of "K_o" on antenna bandwidth.

3.4. Design the CPW to CPS Transition

The second modification for the proposed antenna is to use CPW to CPS transition as shown in Fig. 11.

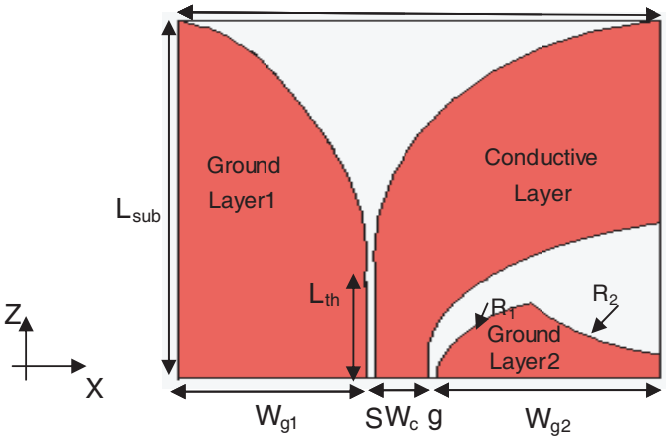

Figure 11. The modified antenna with CPW to CPS transition.

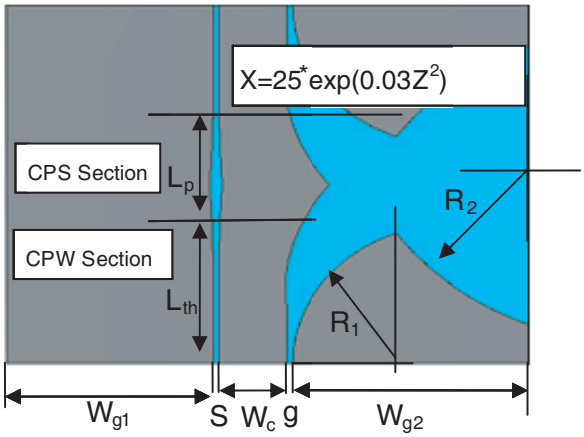

Figure 12. The CPW to CPS transition.

CPW-to-CPS transitions are widely used as feeding for TSA. We simplified the configuration of this transition so as to make it much easier to fabricate and integrate with the antenna. The dimensions of the transition are optimized by CST ver. 2015.

To design the CPW-to-CPS transition, various steps are followed:

(i) The initial values of the CPW parameters (S, W_{g1}, and W_c) may be taken from Table 3.

(ii) Using the initial values to calculate the effective dielectric permittivity $\varepsilon_{\text{reff}}$ and characteristic impedance Z_{coplanar} from the design equation in [9] and iterating until **S, Wc, g achieve** $Z_{\text{coplanar}} = 50\,\Omega$. The proposed back to back transition is shown in Fig. 12.

(iii) For the remaining parameters R_1, R_2, initial values are assumed such that R_1 takes the values between 0 and L_{th}. According to the geometry of the antenna assume R_1 30 mm and $L_{th} = 44$ mm and $R_2 \geq 1.5 * R_1$ to avoid any kind of reflection or coupling with the antenna radiating element.

The selection of the circular shape for the CPW part not selecting exponential rate is due to the need to achieve fast matching within a limited area of extension, so size reduction is achieved.

(i) Simulating the CPW to CPS transition shown in Fig. 12 using CST ver. 15, with the two transitions connected back to back. The size of the model is 200 × 140 mm, as shown in Fig. 11. The initial CPS dimensions are $W_c = 24$ mm and $L_p = 36$ mm. For the CPW, the dimensions are $Wg_1 = Wg_2 = 100$ mm, $S = 2$ mm, and $g = 2.5$ mm. For the two parts of the strip line, one is connected to the CPW ground and the other connected to the CPW central conductor. All the dimensions are optimized to obtain the characteristic impedance of 50 ohm. The optimized values of R_1 and R_2 are 42 mm and 81 mm, respectively, and also the final optimized values for W_c, S and g are 23 mm, 1.5 mm, and 1.9 mm, respectively.

As shown in Fig. 13, the CPW to CPS transition bandwidth is extended from 0.64 GHz to more than 6 GHz.

Figures 14, 15 show the parametric study of R_1 and R_2 when simulating the CPW transition with the antenna. As R_1 increases, the bandwidth is decreased, and the optimum value is $R_1 = 42$ mm. For R_2, the change is slightly small as it increases the lower frequency of the antenna and the optimum value of $R_2 = 81$ mm.

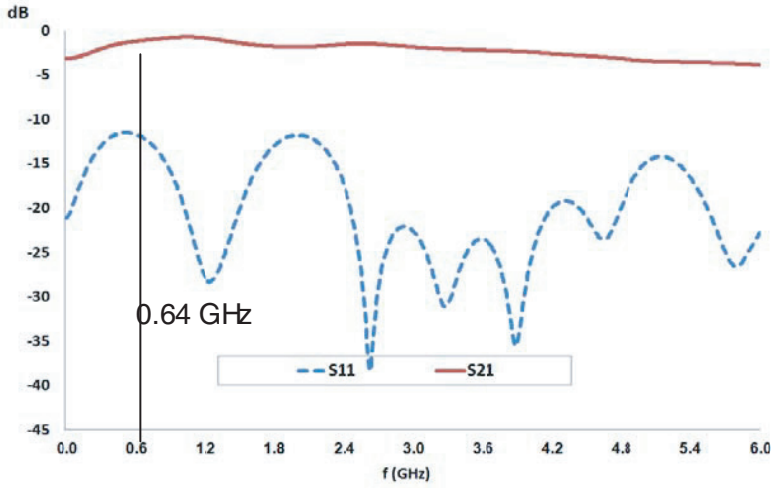

Figure 13. The return losses for the CPW to CPS transition.

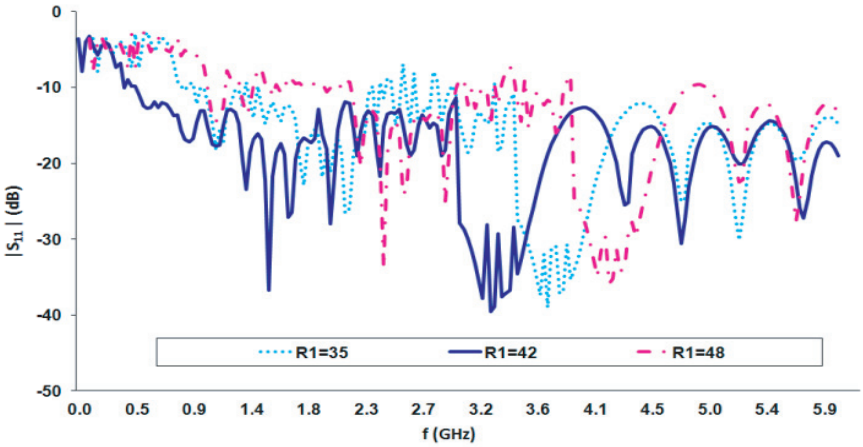

Figure 14. S_{11} versus frequency for different values of R_1 ($R_2 = 75\,\text{mm}$).

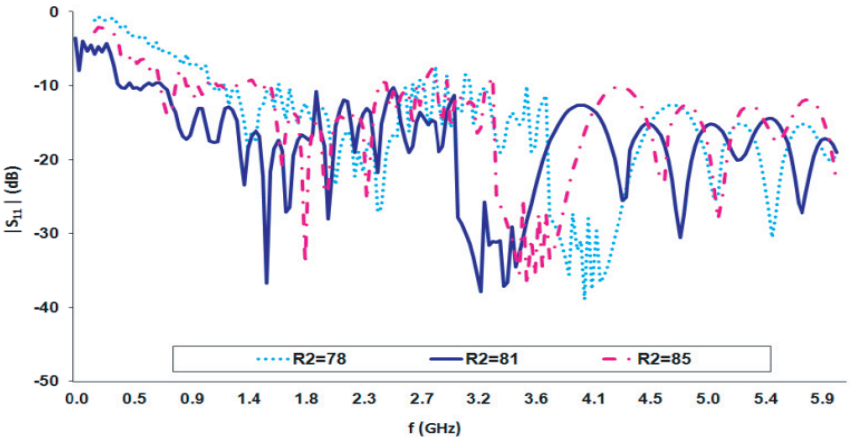

Figure 15. S_{11} versus frequency for different values of R_2 ($R_1 = 42\,\text{mm}$).

3.4.1. Adding Rolled Back Elongated Arm and the Corrugated Structures

The antenna geometry is shown in Fig. 16, with elongated length L_{arm} and two types of slits "corrugated structure" which are the wide slits with widths L_{s1}, L_{s2}, and L_a and the narrow slits with widths L_o and L_r. Table 1 shows the optimized parameters.

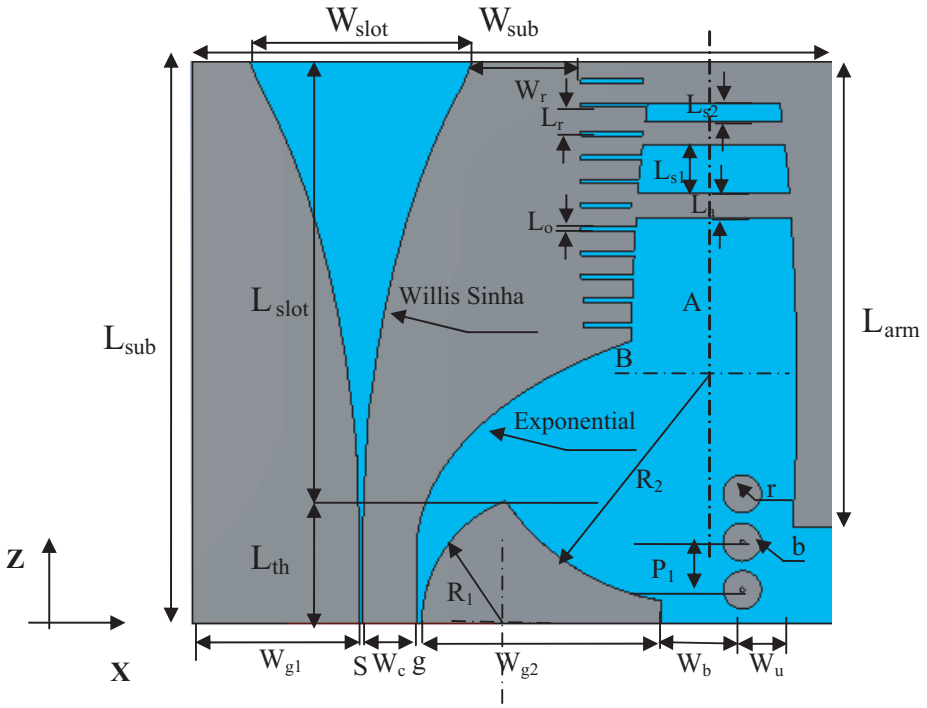

Figure 16. The antenna geometry after adding the rolled arm and corrugated structures.

By adding the elongated arm, the lower end of bandwidth reaches 180 MHz as shown in Fig. 17, i.e., the effect of adding the arm on the frequency band is to shift the minimum frequency from 0.7 GHz to 0.18 GHz. Consequently, a size reduction of 23% is achieved as the substrate length is decreased from 300 to 235 mm, but the effect on the antenna gain is worse as the gain is reduced from 7 dBi to 4 dBi in the GPR frequency of operation from 0.4 to 1.5 GHz as shown in Fig. 18.

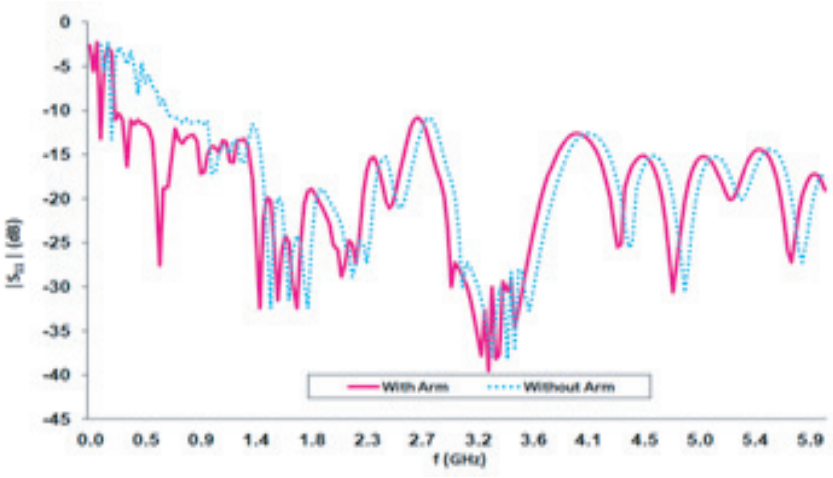

Figure 17. The effect of adding arm on the antenna bandwidth.

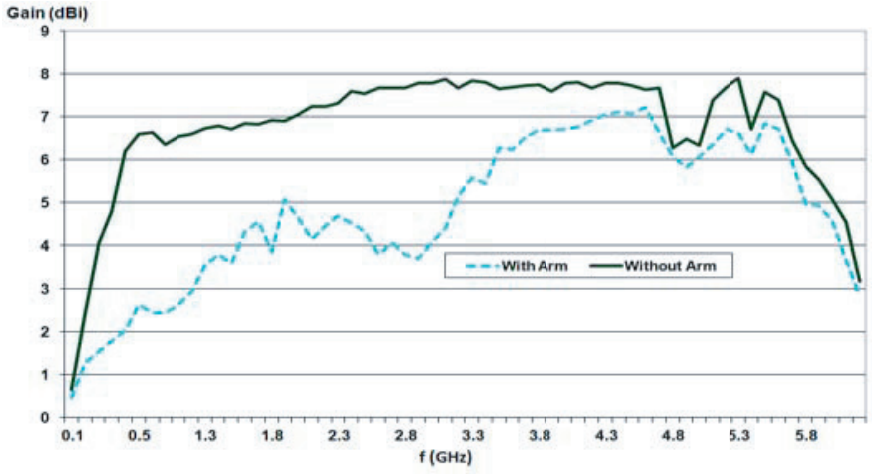

Figure 18. Antenna gain with arm and without arm.

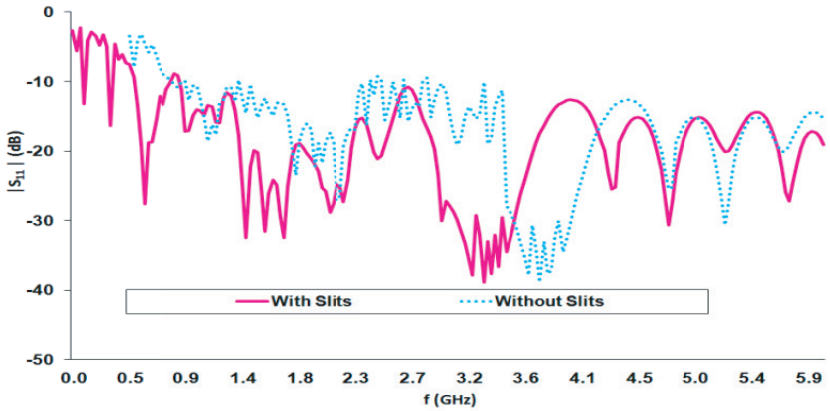

Figure 19. The return loss of the antenna before and after adding Slits.

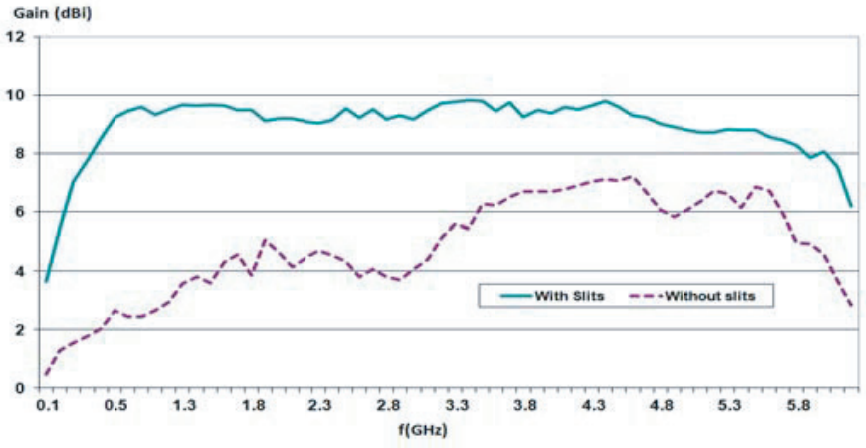

Figure 20. The antenna gain before and after adding slits.

Optimization is performed to enhance the antenna gain and maintain slight change in the lower frequency. Fig. 19 shows the effect of adding slits on antenna bandwidth, and the gain is enhanced after adding the corrugated structure in the outer edge of the antenna element and increased to 9 dBi in the GPR frequency range of operation from 0.4 to 1.5 GHz as shown in Fig. 20.

3.5. Etching Air Cavities inside the Substrates and Its Effect on Antenna Gain and Radiation Efficiency

By making circular air cavities inside the substrate aligned with the tapering profile and antenna outer edge, the antenna average gain is increased from 9 dBi to 11.8 dBi, i.e., the gain is enhanced by 23% as shown in Fig. 21. The simulated radiation efficiency of the proposed antenna is shown in Fig. 22, and the average radiation efficiency in the frequency band 0.4 to 1.5 GHz is equal to 88%.

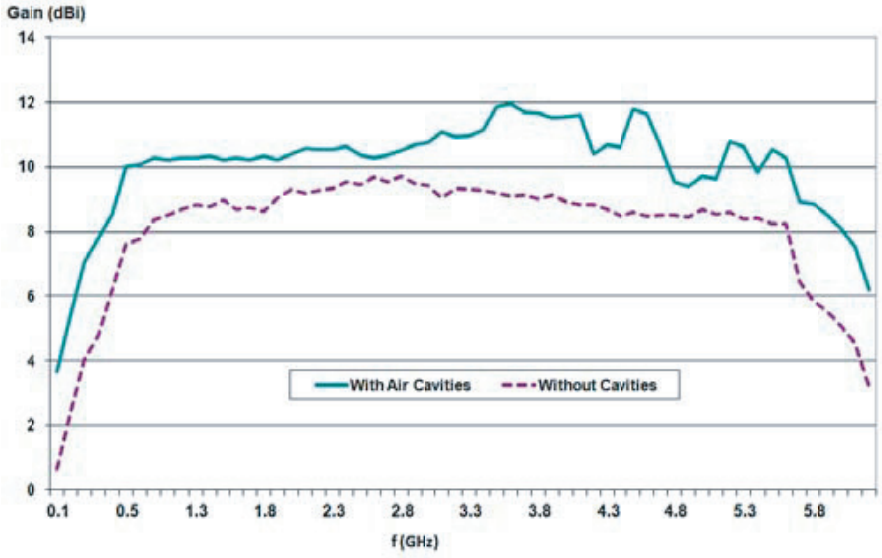

Figure 21. The antenna gain with and without air cavities.

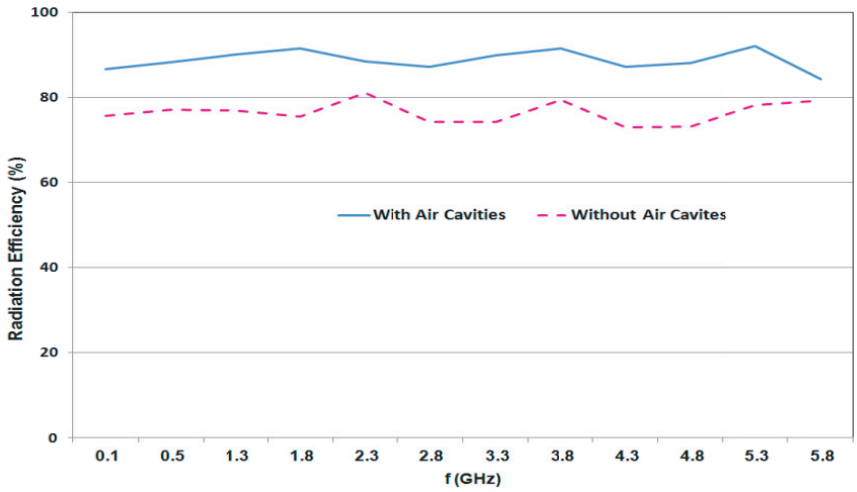

Figure 22. The antenna radiation efficiency with and without air cavities.

The real and imaginary parts of the input impedance vary from 38 to 63 ohm and from 20 to 20 ohm, respectively, as shown in Fig. 23. The simulated and measured S_{11} and VSWR are shown in Fig. 24 and Fig. 25, respectively. There is a good agreement between simulated and measured results. The small discrepancy between their results may be attributed to fabrication tolerances and launcher soldering.

The simulated and measured normalized radiation patterns of the proposed antenna in E-plane

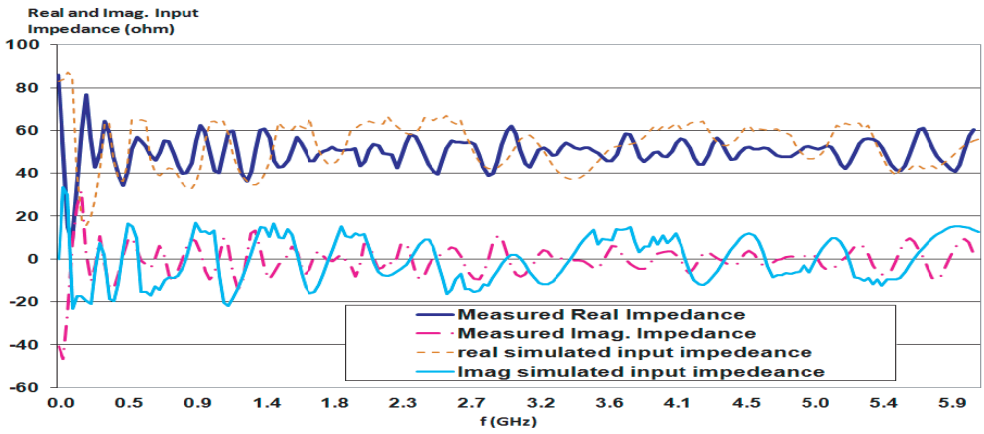

Figure 23. The simulated and measured input impedance against frequency.

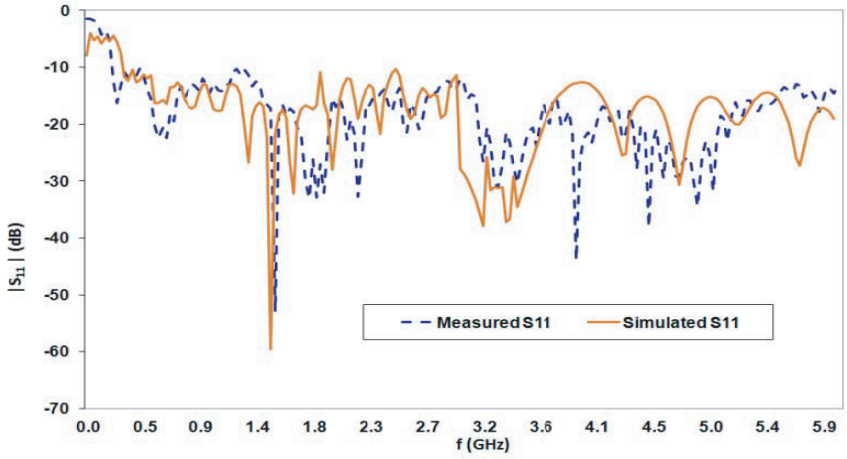

Figure 24. The simulated and measured return loss.

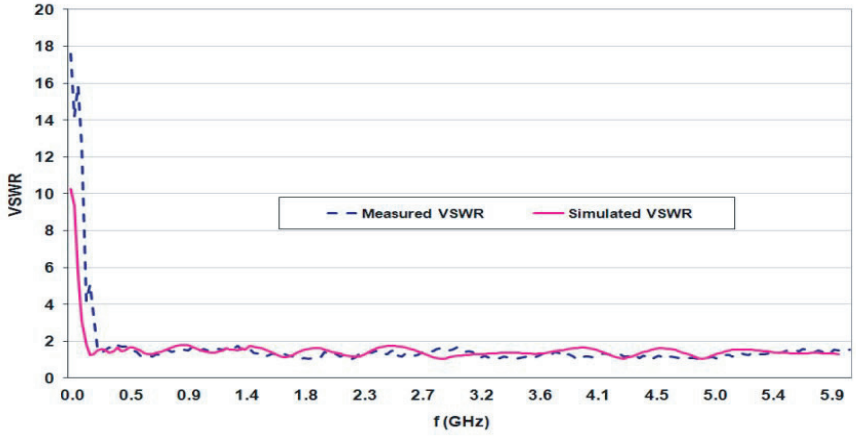

Figure 25. The measured and simulated VSWR.

(yz) and H-plane (xz) at the frequencies of 0.75, 1, and 1.5 GHz are plotted in Fig. 26. As shown in this figure, this design exhibits an end-fire profile in lower frequencies for the xz plane, and the antenna side lobes is almost changed from -17 dB at 0.75 GHz to lower than -30 dB at 1.5 GHz, besides the beam

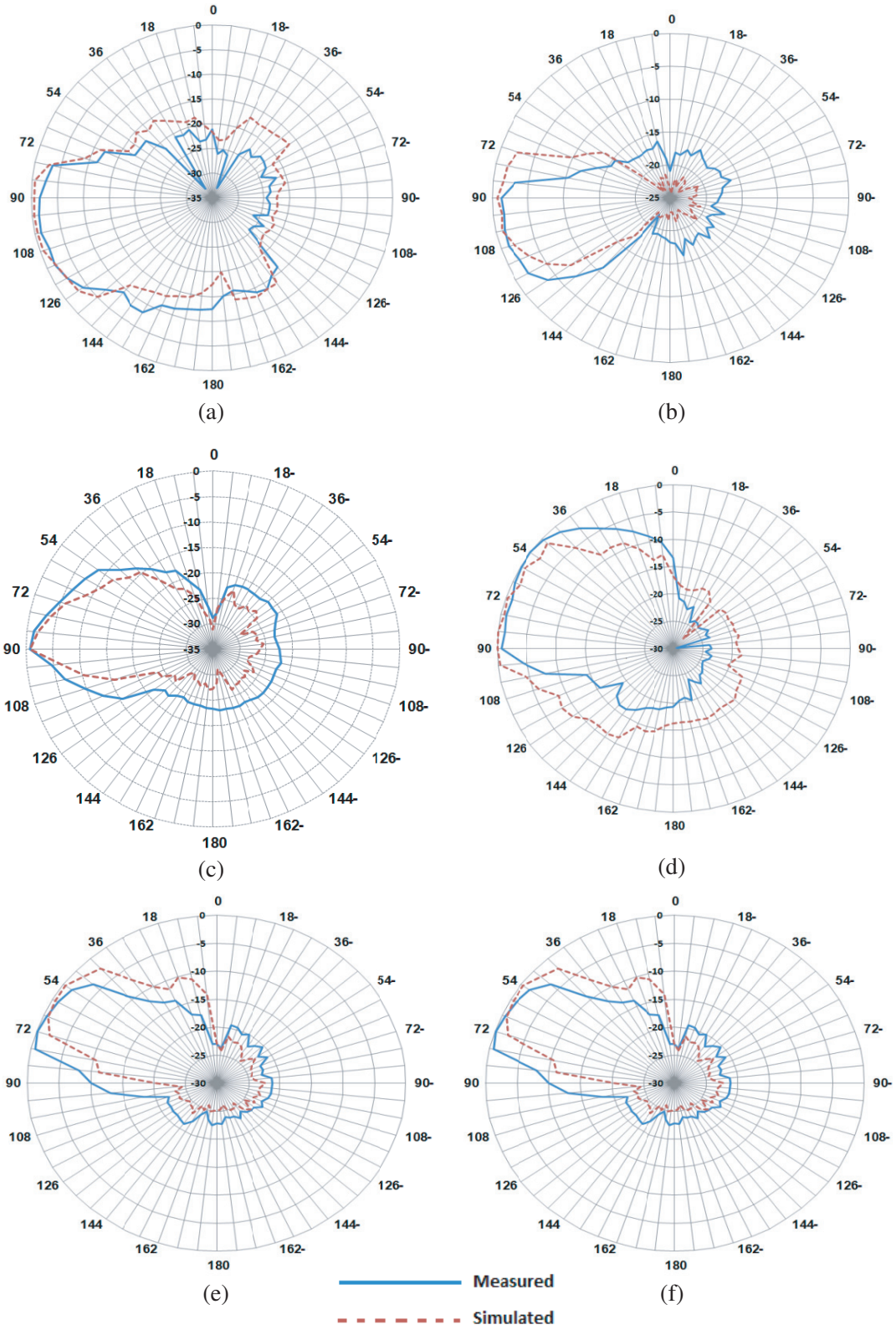

Figure 26. The simulated and measured radiation pattern in the xz plane, (a)–(c) for frequencies 0.75, 1, 1.5 GHz and (d)–(f) in y-z plane for the same frequencies.

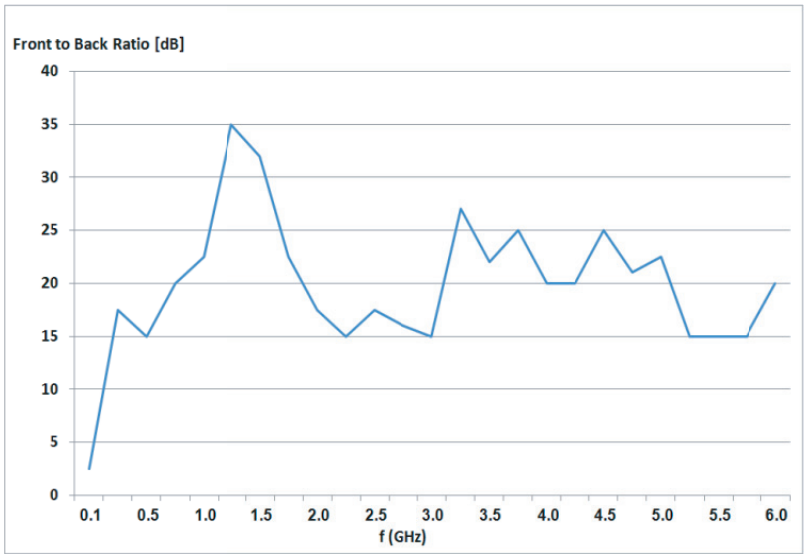

Figure 27. The simulated antenna front to back ratio against frequency.

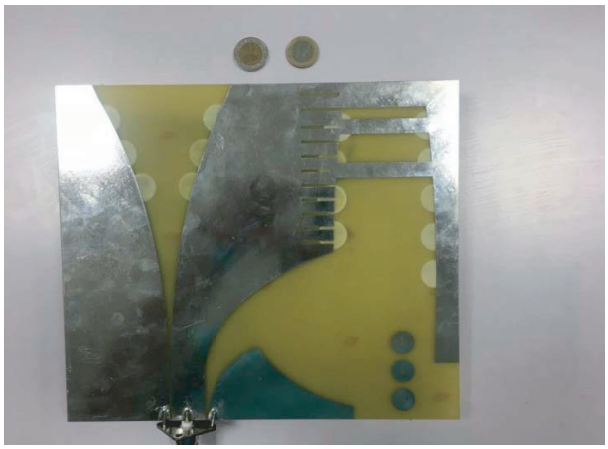

Figure 28. The fabricated antenna.

direction almost near 90° which adds better isolation and directivity for the antenna in GPR application. While in y-z plane the patterns exhibit better stability. Besides, the radiation beam direction changes slightly between 54° to 70° which is reasonably in accordance with the nature of TSA. The antenna directivity is enhanced because the slot width becomes narrow $W_{\text{slot}} = 94\,\text{mm}$.

The average front to back ratio equals 23 dB, i.e., it has good front to back ratio at the lower frequencies, which enhances the antenna directivity as shown in Fig. 27, and the fabricated antenna is shown in Fig. 28.

The modifications summery can be described as in Table 4. In conclusion, the percentages of enhancement in antenna gain and bandwidth due to using CPW to CPS Transition, Corrugated Slits and Cavities are 175% and 287% respectively as shown in Table 4.

Also, comparison between the proposed antenna and the antenna published in [12] is shown in Table 5. Although the proposed antenna size is changed slightly, some enhancements are achieved in the proposed antenna. Firstly, bandwidth is enhanced by 9%, and secondly, the antenna gain is increased by 75% in the GPR frequency band. This enhancement leads to a very good performance for the proposed antenna compared to the published one [12] in GPR system applications.

Table 4. The modification steps for the proposed Willis Sinha antenna.

Item	Average Gain (dBi)	Bandwidth (GHz)
Symmetric Willis Sinha Tapering profile	2.4	1.15
Asymmetric Coplanar Strip Line	4	1.5
Including CPW to CPS transition	7	3.5
Adding arm and slits	9	5.82
Adding cavities	11.8	5.81
Percentage of enhancement due to Transition, Slits and Cavities	195%	287%
Antenna area size reduction	48%	

Table 5. Comparison between the proposed antenna and the published antenna in [12].

Item		Proposed antenna	Published antenna [12]	Difference (%)
Bandwidth (GHz)		6.32	5.78	9%
Lower end of antenna bandwidth (GHz)		0.18	0.22	−22%
Antenna gain in GPR application (0.4–3 GHz) (dBi)		11.8	3	75%
Antenna Size	Width (mm)	270	210	22%
	Length (mm)	235	258	−10%

4. CONCLUSION

A novel uUltra-wideband Willis-Sinha Tapered Slot antenna for landmine detection using Ground Penetrating Radar (GPR) system with enhanced gain and directivity is presented. The operational bandwidth of this antenna extends from 0.18 to 6.2 GHz. The minimum return loss reaches 60 dB. The average directivity reaches 12.2 dBi while the gain and radiation efficiency are 11.8 dBi and 92%, respectively with gain enhancement of 195% due to using corrugated structure and air cavities. The average front-to-back ratio (F/B ratio) is 23 dB. A size reduction of 48% is also achieved due to using extended arm. The antenna performance is simulated and measured. Good agreement is found between numerical and experimental results. The proposed antenna is suitable for various ultra-wideband applications especially in landmine detection.

REFERENCES

1. Huici, M. A. and F. Giovanneschi, "A combined strategy for landmine detection and identification using synthetic GPR responses," *Journal of Applied Geophysics*, Vol. 99, No. 1, 154–165, Dec. 2013.
2. Tsipis, K., "Report on the landmine brainstorming workshop," *Sci. Technol. Int. Security Program*, MIT, Cambridge, MA, 1996.
3. Giannakis, I., A. Giannopoulos, and C. Warren, "A realistic FDTD numerical modeling framework of ground penetrating radar for landmine detection," *IEEE Journal of Selected Topics in Applied Earth Observations and Remote Sensing*, Vol. 9, No. 1, 37–51, Jan. 2016.
4. Sai, B. and L. P. Ligthart, "GPR phase-based techniques for profiling rough surfaces and detecting small, low-contrast landmines under flat ground," *IEEE Trans. Geosci. Remote Sens.*, Vol. 42, No. 2, 318–326, Feb. 2004.

5. Walker, P. D. and M. R. Bell, "Non-iterative techniques for GPR imaging through a non-planar air-ground interface," *IEEE Trans. Geosci. Remote Sens.*, Vol. 40, No. 10, 2213–2223, Oct. 2002.
6. Carin, L., J. Sichina, and J. F. Harvey, "Microwave underground propagation and detection," *IEEE Trans. Microw. Theory Tech.*, Vol. 50, No. 3, 945–952, Mar. 2002.
7. El-Shenawee, M., C. Rappaport, E. L. Miller, and M. B. Silevitch, "Three dimensional subsurface analysis of electromagnetic scattering from penetrable/PEC objects buried under rough surfaces: Use of the steepest descent fast multipole method," *IEEE Trans. Geosci. Remote Sens.*, Vol. 39, No. 6, 1174–1182, Jun. 2001.
8. Shao, J., G. Fang, Y. Ji, K. Tan, and H. Yin, "Design of a low-profile dual exponentially tapered slot antennas," *IEEE Antenna and Wireless Propagation Letters*, Vol. 12, 972–975, 2013.
9. Garg, R., I. Bahl, and M. Bozzi, *Microstrip Lines and Slot Lines*, 3rd Edition, 2013.
10. Abuhalima, S., E. Abdallah, and D. Mohamed, "Ultra wideband elliptical microstrip antenna using different taper lines for feeding," *11th WSEAS International Conference on Communications*, 144–149, Greece, Jul. 26–28, 2007.
11. Mao, S. G., C. T. Hwang, R. Wu, and C. H. Chen, "Analysis of coplanar waveguide-to-coplanar stripline transitions," *IEEE Trans. on Antennas and Propag.*, Vol. 48, No. 1, 23–29, Jan. 2000.
12. Zhang, F., G. Y. Fang, Y. J. Ju, and J.-J. Shao, "A novel compact double exponentially tapered slot antenna (DETSA) for GPR applications," *IEEE Trans. Antennas Propag.*, Vol. 11, 195–198, 2011.
13. Wang, Z. and H. Zhang, "Improvement in a high gain UWB antenna with corrugated edges," *Progress In Electromagnetics Research C*, Vol. 6, 159–166, 2009.
14. Moosazadeh, M. and S. Kharkovsky, "A compact high-gain and front-to-back ratio elliptically tapered antipodal vivaldi antenna with trapezoid-shaped dielectric lens," *IEEE Antennas and Wireless Propagation Letters*, Vol. 15, 552–555, 2016.
15. Liu, Y., W. Zhou, S. Yang, W. Li, P. Li, and S. Yang, "A novel miniaturized vivaldi antenna using tapered slot edge with resonant cavity structure for ultrawideband applications," *IEEE Antennas and Wireless Propagation Letters*, Vol. 15, 1881–1884, 2016.
16. Omar, S. A., A. Iqbal, O. A. Saraereh, and A. Basir, "An array of M-shaped Vivaldi antennas for UWB applications," *Progress In Electromagnetics Research Letters*, Vol. 68, 67–72, 2017.
17. Yeap, S. B. and Z. N. Chen, "Microstrip patch antennas with enhanced gain by partial substrate removal," *IEEE Trans. Antennas and Propagation*, Vol. 58, No. 9, 2811–2816, Sept. 2010.
18. Grigorievich, T., L. Kempen, H. Sahli, J. Sachs, and M. Sato, "Investigation of time-frequency features for GPR landmine discrimination," *IEEE Trans. on Geosciences and Remote Sensing*, Vol. 45, No. 1, 118–129, Jan. 2007.
19. Cohn, S. B., "Slot line on a dielectric substrate," *IEEE Trans. Microwave Theory Techniques*, Vol. 17, 768–778, Oct. 1969.
20. Abbosh, A., "Gain and bandwidth optimization of compact UWB tapered slot antennas," *International Journal of Microwave and Optical Technology*, Vol. 2, No. 3, 222–225, 2007.